ACS OMEGA

http://pubs.acs.org/journal/acsodf

Article

Chitosan–Terephthalic Acid–Magnetic Composite Beads for Effective Removal of the Acid Blue Dye from Aqueous Solutions: Kinetics, Isotherm, and Statistical Modeling

Caroline Avosuahi Akinremi, Abideen Idowu Adeogun,* Maxime Poupin, and Katherine Huddersman

Cite This: *ACS Omega* 2021, 6, 30499–30514

Read Online

ACCESS | Metrics & More | Article Recommendations

ABSTRACT: A terephthalic acid-modified chitosan–magnetic nanocomposite (Cs–Tp@Fe_3O_4) was synthesized and characterized. The synthesized Cs–Tp@Fe_3O_4 was used in a batch process for the adsorptive removal of the acid blue 25 (AB-25) dye in aqueous solutions. The kinetic data were subjected to the pseudo-first-order, pseudo-second-order, Elovich, and intra-particle diffusion models, while the equilibrium data were evaluated with the Langmuir, Freundlich, Temkin, and Dubinin–Radushkevich isotherm models. The effects of the initial dye concentration, contact time, and adsorbent dosage, as well as their interactions, on the removal efficiency were investigated using the design of experiments based on a central composite design, and the resultant data were modeled with the response surface methodology (RSM), artificial neural network (ANN), adaptive neuro-fuzzy inference system (ANFIS), and multiple linear regression (MLR) approaches. The adsorption process followed pseudo-first-order with good agreement between the experimental $Q_{e(exp)}$ and calculated $Q_{e(cal.)}$ amounts of dye adsorbed, as well as the values of correlation coefficient, R^2 (0.999) and percentage of sum square error, % SSE (0.640). All the investigated adsorption isotherms fitted all models well in the order of Dubinin–Radushkevich > Langmuir > Freundlich > Temkin with R^2 > 0.9 with the monolayer maximum adsorption capacity of 440.24 mg/g obtained from the Langmuir isotherm. The RSM model predicted the maximum removal efficiency at an optimum initial dye concentration of 19.11 mg/L, a contact time of 95.3 min, and an adsorbent dosage of 0.18 g. Statistically, the models were fitted in the order of RSM > ANN > ANFIS > MLR. These results indicated that the prepared Cs–Tp@Fe_3O_4 is an efficient adsorbent for the AB-25 dye removal with excellent stability for water treatment applications.

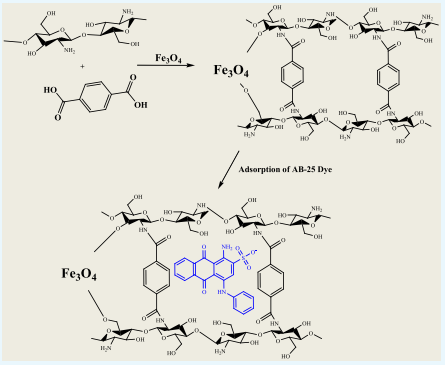

INTRODUCTION

Untreated industrial effluents are highly loaded with recalcitrant xenobiotics including dyes, surfactants, as well as other organic and inorganic pollutants. The single largest cause of the paucity of freshwater in most third world countries can be attributed to pollution by industrial effluents and sewages.[1] The major sources of colored wastewater in the environment are from dye manufacturers and their consumers, which include textile, leather, plastic, paper, cosmetic, pharmaceutical, and food industries.[2,3] Most chemical compounds in industrial effluents, but especially the synthetic dyes, even at minute concentrations pose not only a health hazard but also can destroy the esthetic nature of the water system by reducing the photosynthetic activity and thus decreasing the recreation activities of the stream as a whole.[3,4] Also, in addition to their unacceptable appearance and the toxic effects of dyes and that of the products of their degradation, the nearby soil, sediments, and surface water may be contaminated, thus becoming a major global environmental pollution challenge.[5] Acid blue 25 ($C_{20}H_{13}N_2NaO_5S$, AB-25) is a synthetic anionic acid dye with an anthraquinone structure. It is used in a lot of products as a colorant, for example, household cleaning agents, personal care products, textile dyes, drugs, inks for printing, and so forth. As a synthetic dye, it is non-biodegradable and harmful with persistent effects when discharged into the environment, especially to aquatic life.[6,7] The treatment of dye-containing effluents is necessary to protect the ecosystem; also, reusability of recovered water for irrigation purposes and other industrial purposes are both eco-friendly and sustainable.

Remediation of dye contamination wastewater to reduce their ecological consequences has attracted several physical, biological, and chemical techniques. The adsorption method had been the most extensively studied physico-chemical treatment and had proved to be of potential application. It is of low cost, effective, and highly efficient; however, the major drawback is

Received: July 25, 2021
Accepted: October 15, 2021
Published: November 5, 2021

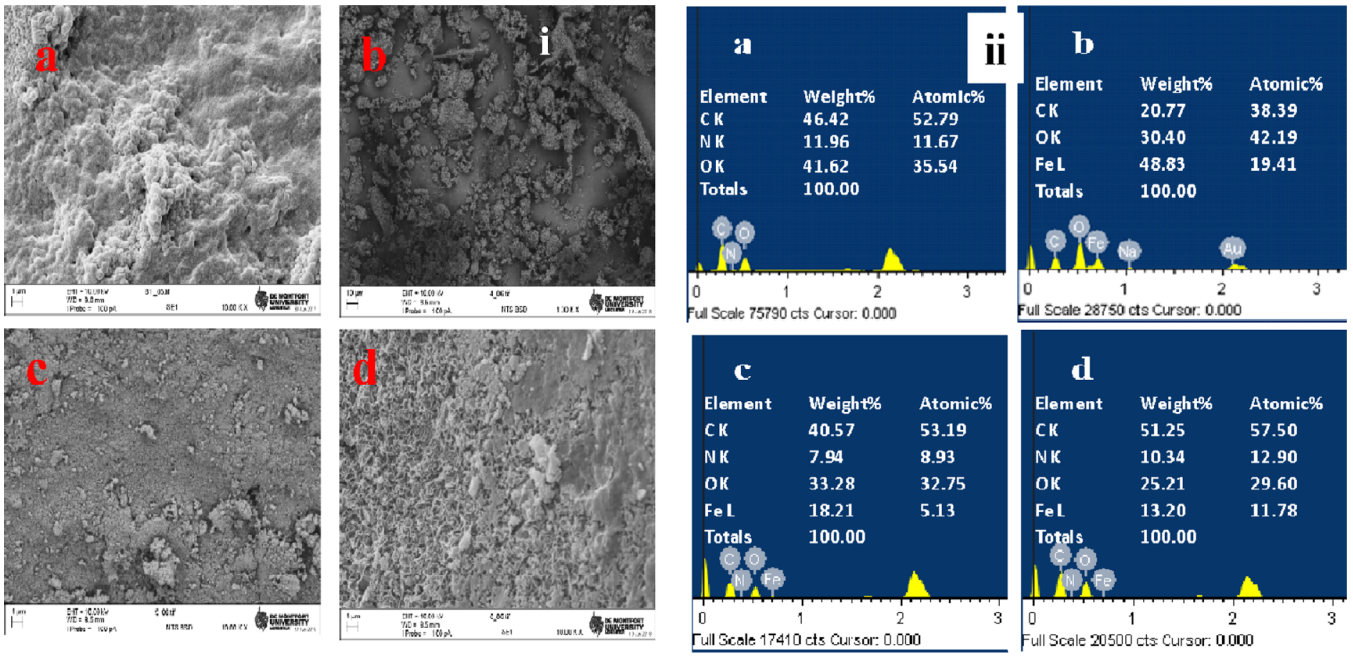

Figure 1. (i) SEM images and (ii) EDX and elemental analyses of: (a) Cs, (b) Fe_3O_4, (c) Tp@Fe_3O_4, and (d) Cs−Trp@Fe_3O_4.

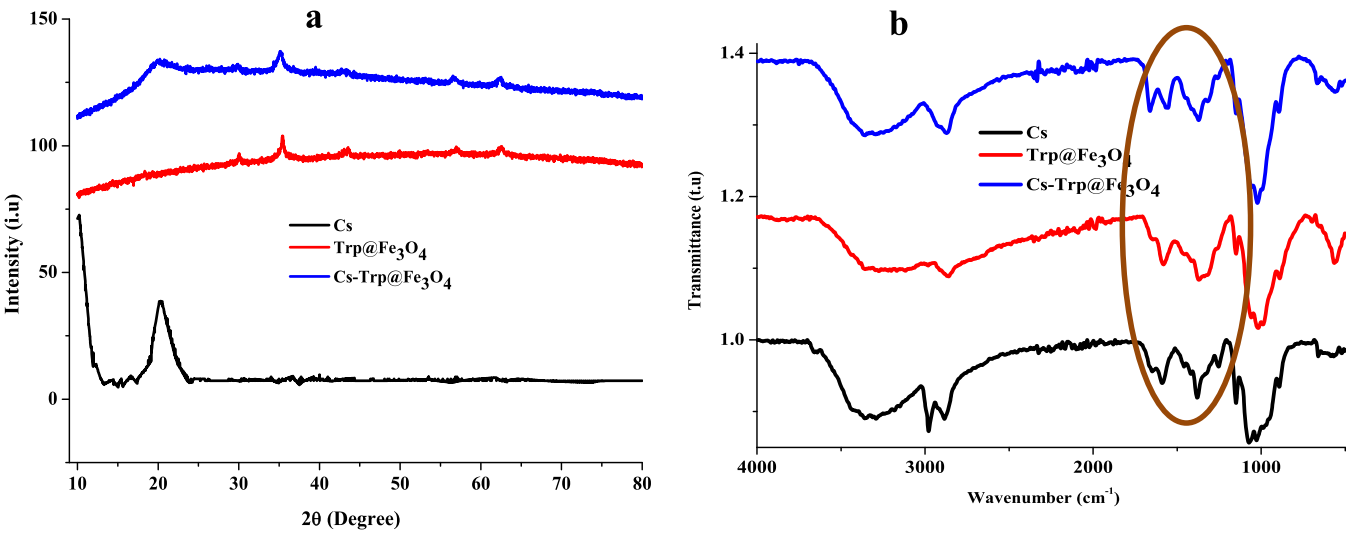

Figure 2. (a) XRD patterns and (b) FTIR spectra of chitosan, Tp@Fe_3O_4, and Cs−Tp@Fe_3O_4.

the selection of the adsorbent.[8] Activated carbon has significant adsorption capacity and had been widely accepted as the best adsorbent in commercial systems; unfortunately, the high capital cost, complicated synthesis process, slow kinetic properties, and difficulties in regeneration which is usually performed off-site and with limited success are major impediments to its application; thus, researchers have sought other more efficient and cost-effective adsorbents.[9−11]

Chitosan, a natural polysaccharide obtained from the chitin biopolymer through N-deacetylation has been a focus for the development of a low-cost biopolymer-based adsorbent. It has been found to be an effective adsorbent compared to activated carbon with its high adsorption potential attributed to the presence of hydroxyl and amino functional groups.[12] These groups have potential for electrostatic interactions upon protonation in an acidic medium,[8,13] thus conferring outstanding properties to chitosan. Interest in chitosan is also connected with its attractive properties such as biodegradability, low toxicity, and biocompatibility, coupled with the availability of natural resources required for its chemical and enzymatic modifications for specific end uses.[14,15] Though chitosan is a highly effective adsorbent for the removal of a variety of pollutants, its poor mechanical properties, low thermal stability, insufficient solubility in dilute acids, as well as its relatively low surface area are major setbacks in its application.[16] As a means of overcoming these challenges, its modification with other composites had been the focus of investigation.[17] Thus, materials such as cellulose and its derivatives, clay materials including bentonite, zeolites, and so forth, as well as metal−organic frameworks, conducting polymers, and other polymeric materials had been investigated.[8,15]

Another important drawback for chitosan application as an adsorbent is the inability of simple separation techniques (i.e., filtration or sedimentation) to remove it from aqueous media

https://doi.org/10.1021/acsomega.1c03964
ACS Omega 2021, 6, 30499−30514

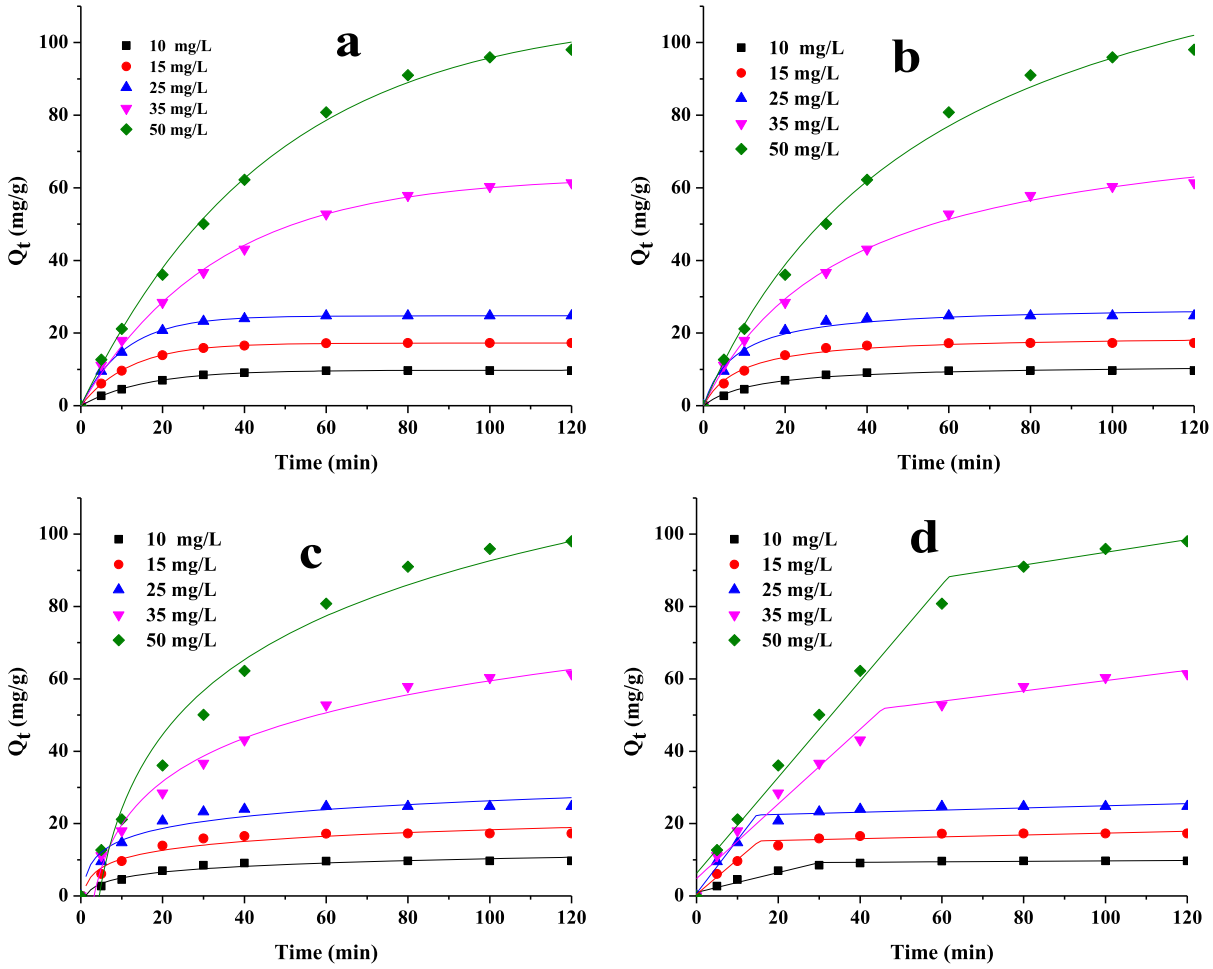

Figure 3. Kinetic model fits for the removal of AB-25 by Cs−Tp@Fe_3O_4: (a) pseudo-first-order, (b) pseudo-second-order, (c) Elovich, and (d) intra particle diffusion for different initial concentrations of AB-25.

after the adsorption process, leading to filter blockage and loss of adsorbent. Thus, coating chitosan or its composite on magnetic materials for easy separation of the adsorbent had been suggested. Magnetite (Fe_3O_4) and maghemite (Fe_2O_3) are among the magnetic materials that had been extensively studied due to their strong super-paramagnetic activity, facile preparation, high thermal stability, as well as low toxicity. Coating these magnetic particles with chitosan materials also reduces their sensitivity to solubilization by acidic environments; thus, their attenuation is enhanced with improved performance for effective separation from aqueous media.

This study investigated the potential of chitosan/terephthalic acid-coated magnetic nanoparticles for the removal of an acid blue dye. The combined effects of pH, contact time, and initial dye concentration were investigated using the response surface methodology (RSM), artificial neural network (ANN), and adaptive neuro-fuzzy inference system (ANFIS) methodologies based on data obtained from a central composite design of experimental approach. Kinetic and equilibrium data from the batch adsorption studies were subjected to analysis by appropriate models.

RESULTS AND DISCUSSION

Characterizations of the Adsorbent. The synthesized adsorbent was characterized by scanning electron microscopy (SEM), energy-dispersive X-ray (EDX) analysis, X-ray diffraction (XRD), and Fourier transform infrared (FTIR) spectroscopy to confirm the compositions of the adsorbent. The SEM images (Figure 1i) reveal the intergranular porous structure of the materials with amorphous morphologies of different particle sizes. Figure 1ia reveals the uneven texture of the chitosan bead, while the rough and agglomerate morphology of the magnetic nanoparticle is displayed in Figure 1ib. The porous and evenly distributed grain size and some agglomeration of the magnetic particles within terephthalic acid are revealed in Figure 3ic. The surface morphology of Cs−Tp@Fe_3O_4 beads (Figure 1id) revealed a distinct surface different from those of the component precursors; the smooth surface and the agglomerated rough surface of the chitosan and Tp@Fe_3O_4, respectively, had been transformed to a well-formed crater, indicating the formation of the Cs−Tp@Fe_3O_4composite.

Figure 1ii depicts the result of EDX and elemental analyses of chitosan, Fe_3O_4, its terephthalic acid composite, as well as the Cs−Tp@Fe_3O_4 composite. The elemental analysis of chitosan (Figure 1iia) shows the major components as C, O, and N, while Figure 3iib reveals the proportion of Fe and O in the magnetic particles. The C content of the adsorbent (Figure 1iid) is considerably higher than that of the entire precursor components, confirming the synthesis of the adsorbent with potential for high adsorption efficiency. The retention of Fe in

https://doi.org/10.1021/acsomega.1c03964
ACS Omega 2021, 6, 30499−30514

Table 1. Kinetic Parameters for the Adsorption of AB-25 by Cs−Trp@Fe_3O_4

C_o (mg/L)	10	15	25	35	50
Pseudo-First-Order Kinetics Model Parameters					
Q_{eexp} (mg g^{-1})	9.700	17.225	24.750	61.400	98.051
Q_{ecal}(mg g^{-1})	9.773	17.231	24.740	63.137	108.259
k_1 (min^{-1})	0.064	0.083	0.093	0.030	0.022
R^2	0.999	0.999	0.999	0.999	0.999
SSE	5.66×10^{-5}	1.21×10^{-7}	1.63×10^{-7}	8.00×10^{-4}	1.08×10^{-2}
AIC	−116.821	−178.301	−175.321	−90.335	−64.308
AICc	−115.107	−176.586	−173.607	−88.621	−62.594
BIC	−113.913	−175.393	−172.413	−87.427	−61.400
HQIC	−119.153	−180.633	−177.653	−92.667	−66.640
RMSE	1.51×10^{-3}	6.97×10^{-5}	8.08×10^{-5}	5.66×10^{-3}	2.08×10^{-2}
HYBRID	0.003	0.001	0.002	0.113	0.416
Pseudo-Second-Order Kinetics Model Parameters					
Q_{ecal} (mg g^{-1})	11.307	19.384	27.567	81.565	151.123
$k_2 \times 10^3$ (g mg^{-1} min^{-1})	6.890	5.710	4.610	0.346	0.115
R^2	0.984	0.987	0.986	0.998	0.995
SSE	0.018	0.012	0.011	0.051	0.080
AIC	−59.200	−63.254	−64.124	−48.785	−44.283
AICc	−57.485	−61.540	−62.410	−47.071	−42.569
BIC	−56.292	−60.347	−61.217	−45.877	−41.375
HQIC	−61.532	−65.586	−66.456	−51.117	−46.615
RMSE	0.027	0.022	0.021	0.045	0.057
HYBRID	0.543	0.444	0.410	0.904	1.135

the final product confirmed the presence of Fe_2O_3 in the nanoparticles.

Figure 2a shows the XRD pattern of the naked Cs, Tp@Fe_3O_4, and the Cs−Tp@Fe_3O_4composite synthesized. The figure reveals the amorphous nature of the naked chitosan with the characteristic peaks at 2θ values of 11.1 and 20.2°. The peak positions of Fe_3O_4 nanoparticles are unchanged in Tp@Fe_3O_4, which illuminates the fact that the binding process did not result in the phase change of Fe_3O_4. The peak intensity of Cs−Tp@Fe_3O_4 composite particles is lower than that of Tp@Fe_3O_4nanoparticles due to the incorporation into Cs microspheres.

The FTIR spectra of chitosan, Tp@Fe_3O_4, and Cs−Trp@Fe_3O_4beads are shown in Figure 2b. The characteristic broad peak at around 3400 cm^{-1} corresponding to the stretching vibrations of OH and NH bonds[18] is pronounced in chitosan in comparison to Tp@Fe_3O_4 and is again pronounced in Cs−Tp@Fe_3O_4, suggesting that the chitosan has been incorporated in the Tp@Fe_3O_4 bead. Furthermore, the peaks at 2890 and 1378 cm^{-1} were both attributed to the C−H stretching vibration of the alkyl group, while those at 1650 and 1590 cm^{-1} were the typical bending vibration bands of primary amino groups of chitosan.[19] The absorption bands at approximately 1020 cm^{-1} were due to the stretching vibration of C−OH bonds present in all the samples.[8] The little difference in the spectrum noticed in the circled area indicates the successful coating of chitosan on Trp@Fe_3O_4.

Adsorption Kinetics Studies. The rates of adsorption of the AB-25 dye at the adsorbent/solution interface were subjected to analysis by the kinetic model eqs 4−7 in order to elucidate the mechanism, the potential removal rate, as well as the diffusion rate-controlling steps affecting the surface reaction and to characterize the effect of activated chemisorption on the adsorption kinetics. The kinetic model fits for the removal of AB-25 by Cs−Tp@Fe_3O_4 are presented in Figure 3a−d, while the corresponding parameters are also shown in Tables 1 and 2.

Table 2. Kinetic Parameters for the Mechanism of Adsorption of AB-25 by Cs−Trp@Fe_3O_4

Elovich's Model Parameters					
α (mg (g min)$^{-1}$)	1.997	6.331	12.147	5.391	6.657
β (g mg^{-1})	0.434	0.284	0.211	0.058	0.034
R^2	0.956	0.948	0.944	0.989	0.974
SSE	0.545	2.634	6.107	0.399	0.622
AIC	−25.096	−9.341	−0.931	−28.214	−23.774
AICc	−23.381	−7.627	0.783	−26.500	−22.060
BIC	−22.188	−6.433	1.976	−25.306	−20.866
HQIC	−27.427	−11.673	−3.263	−30.546	−26.106
RMSE	0.148	0.325	0.494	0.126	0.158
HYBRID	2.953	6.492	9.885	2.527	3.155
Intra-Particle Diffusion Model Parameters					
K_{1d} (mg g^{-1} $min^{-0.5}$)	0.990	0.429	0.708	4.806	6.237
C_1 (mg g^{-1})	0.273	0.963	1.475	1.032	1.329
R^2	0.947	0.964	0.969	0.971	0.980
SSE	0.034	0.014	0.688	1.647	1.353
AIC	−52.840	−61.713	−22.766	−14.036	−16.003
AICc	−51.126	−59.999	−21.051	−12.322	−14.288
BIC	−49.932	−58.805	−19.858	−11.129	−13.095
HQIC	−55.172	−64.045	−25.097	−16.368	−18.335
RMSE	0.065	0.041	0.293	0.454	0.411
HYBRID	1.348	0.260	1.285	1.318	0.976
K_{2d} (mg g^{-1} $min^{-0.5}$)	9.040	14.828	21.962	45.350	77.339
C_2 (mg g^{-1})	0.007	0.025	0.029	0.142	0.177
R^2	0.947	0.964	0.969	0.971	0.980
SSE	0.022	0.046	0.743	0.002	0.095
AIC	−57.193	−49.817	−21.996	−81.172	−42.565
AICc	−55.479	−48.103	−20.282	−79.458	−40.850
BIC	−54.285	−46.909	−19.089	−78.264	−39.657
HQIC	−59.525	−52.149	−24.328	−83.504	−44.897
RMSE	0.053	0.076	0.305	0.016	0.109
HYBRID	0.631	0.307	0.944	0.035	0.218

https://doi.org/10.1021/acsomega.1c03964
ACS Omega 2021, 6, 30499−30514

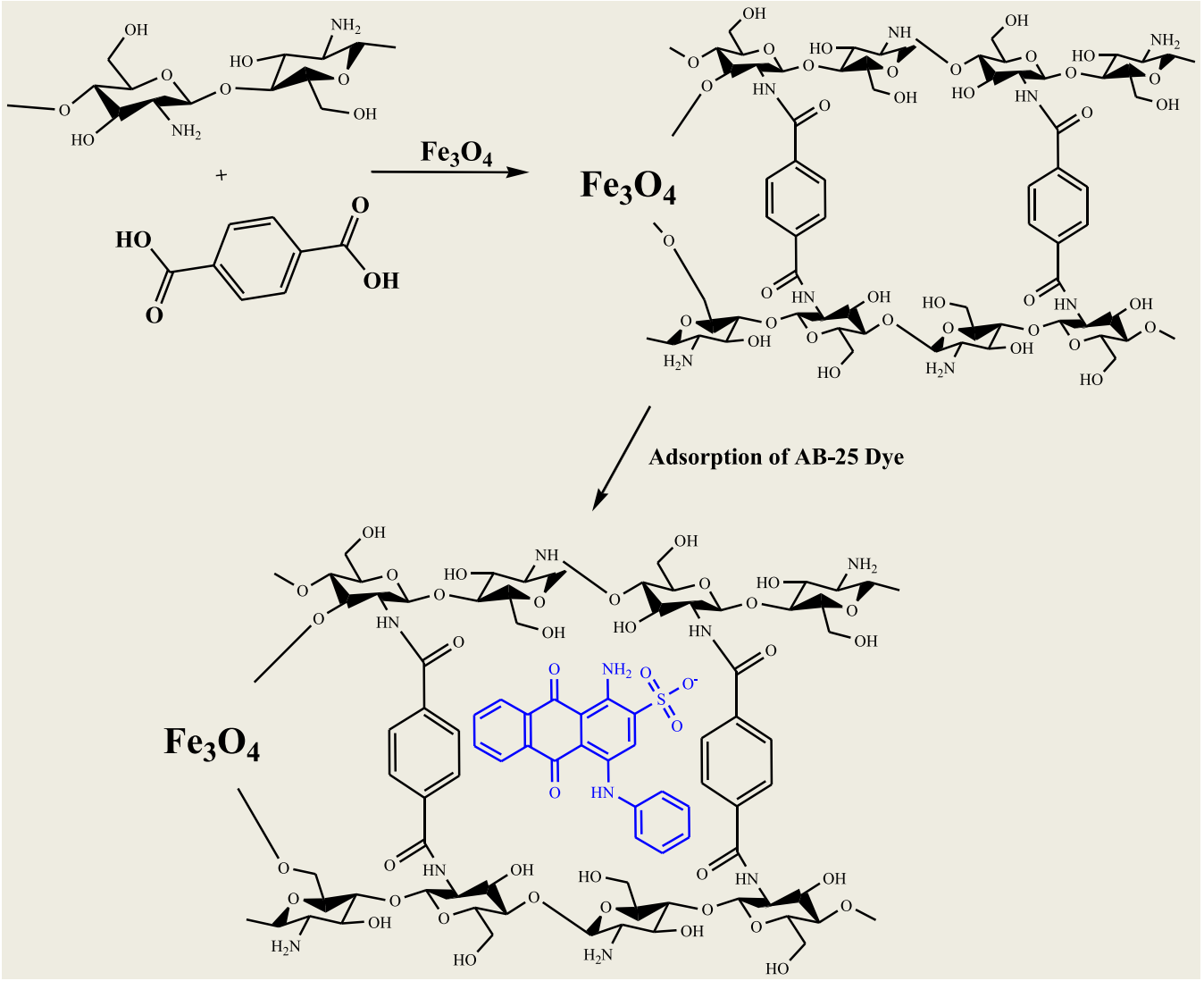

Figure 4. Interaction of AB-25 with Cs−Trp@Fe_3O_4.

The pseudo-first-order adsorption kinetics displayed a correlation coefficient R^2 of 0.999 with the experimental values of Q_e on a par with the calculated values at all concentrations investigated; the pseudo-second-order parameter, on the other hand, has R^2 ranging between 0.984 and 0.998, but the experimental values of Q_e differ slightly from the calculated values when compared with what was obtained from pseudo-first order. The overall analysis of the error functions showed that the adsorption process for this adsorbent is best explained by the pseudo-first-order kinetic model as it has the lowest error values. Similarly, based on the information criterion (IC) values obtained, the Akaike IC (AIC), a version of AIC (AICc), Bayesian IC (BIC), and Hannan−Quinn IC (HQIC) showed that the first-order kinetics model can be conveniently selected, and it ranked higher than the second-order model because of the overall lowest negative values obtained for the model. The increase in the first-order rate constant k_1 with concentration is due to the increase in electrostatic interactions between the adsorbent and the dye molecule as the increase in the driving force across the boundary forced the molecule into the pores and increased the diffusion gradients toward the adsorbent. Also, it is likely that as the concentration of the dye increases, there are less water molecules to solvate the dye molecules allowing adsorbent−dye interactions to become more dominant.

Although the error function is significant, the Elovich model fitted the kinetic data satisfactorily (4Figure 5c) with $R^2 > 0.9$, as shown in Table 2. A decrease in the value of β (a factor related to surface coverage) with the corresponding increase in α (adsorption rate) as the dye concentration increases confirms ion exchange as one of the mechanisms of adsorption process, that is, the rate of dye adsorption increases as the dye concentration increases, and that the adsorbent−dye interaction becomes dominant as the dye concentration increases. The intraparticle diffusion model revealed a two-step mechanism (Figure 3d), and the value of the intercept C_i indicated that film diffusion is insignificant, and that intraparticle diffusion is not the sole determinant of the adsorption mechanism. From the values obtained, the mechanism of adsorption of AB-25 by Cs−Trp@Fe_3O_4 is better assigned to the intraparticle diffusion model, owing to the overall lowest negative values of IC obtained for the model.

Adsorption Isotherms. The interactions between the dye molecule and the adsorbent are depicted in Figure 4. An understanding of the basic properties and interactions of the adsorbent with the adsorbing molecules can be gained through

https://doi.org/10.1021/acsomega.1c03964
ACS Omega 2021, 6, 30499−30514

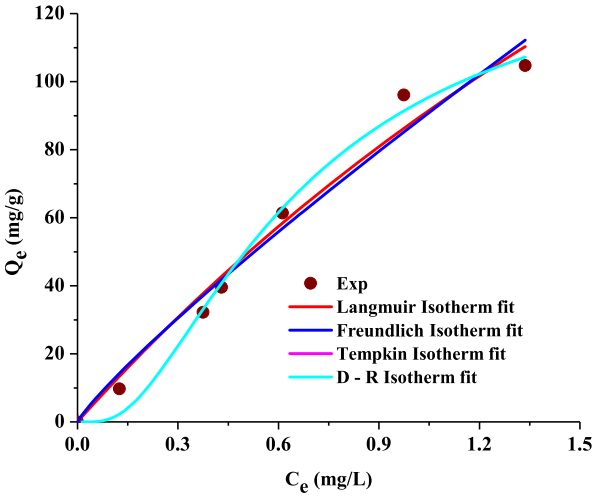

Figure 5. Isotherm fits for the adsorption of AB-25 removal by Cs−Trp@Fe_3O_4.

the parameters determined from the isotherm studies. Figure 5 shows the isotherm fits for the adsorption of AB-25 onto Cs−Tp@Fe_3O_4, while the fitting parameters are presented in Table 3. Based on the regression coefficient R^2, we can find that there is good agreement between the experimental and theoretical data for the different models. The Langmuir isotherm which is based on monolayer adsorption predicts a large maximum adsorption capacity (Q_o) of 440.2 mg $g^{-1}$when compared with other adsorbents, as shown in Table 4, with the separation factor R_L of 0.162, confirming a favorable adsorption of AB-25 onto Cs−Tp@Fe_3O_4.

The Langmuir constant K_L has also been related to the Gibbs free energy (ΔG^o) of sorption as $\Delta G^\circ = -RT \ln (K^o)$, where $K^o = 55.5\ (K_L\ MW_{(dye)})$, to resolve the unit issue.[19] Thus, the ΔG° value of −39.221 kJ mol^{-1} obtained in this study confirmed the feasibility of the process and the spontaneous nature of adsorption. The surface heterogeneity of the adsorbent and the moderately high interactions between the dye and the adsorbent molecule are predicted by the Freundlich and Temkin isotherm parameters. The value of $R^2 > 0.9$ is a clear indication of a good fit by all the isotherms; also, based on the IC values obtained, the AIC, AICc, BIC, and HQIC showed that the models can be conveniently selected and ranked in the order of Dubinin−Radushkevich > Langmuir > Freundlich > Temkin. The sorption energy of less than 1.6 kJ mol^{-1} obtained from the Dubinin−Radushkevich model showed that the adsorption of AB-25 on the adsorbent is through physisorption and an endothermic process; it also suggested a film diffusion-controlled ion-exchange mechanism for adsorption.

Statistical Evaluations. *RSM Study.* Table 5 represents the data from the face central composite (FCC) design of experiment, it consists of 32 experimental runs, with the pH, contact time, and adsorbent dosage being independent variables and the removal efficiency (%)the dependent variable. A response surface regression model and 3D contour plots (Figure 6) were generated from the data based on the quadratic model in eq 1, while the statistical analysis results of the model by ANOVA is given in Table 6. The *F*-values represent the significance of the relevant term; while the statistical significance of the regression model is proven with *p*-values < 0.05, the high sum of squares implies the significance of the variables.[27]

Table 3. Isotherm Models Applied for the Adsorption of AB-25 Removal by Cs−Trp@Fe_3O_4

isotherm	parameter	value
Langmuir	Q_o (mg g^{-1})	440.240
	K_L (g mg^{-1})	0.250
	R_L	0.162
	R^2	0.977
	ΔG° (kJ mol^{-1})	−39.221
	RSSE	189.764
	AIC	27.099
	AICc	30.099
	BIC	28.937
	HQIC	24.431
Freundlich	K_F (g mg^{-1} $min^{-1/n}$)	87.139
	N	1.149
	R^2	0.970
	RSSE	244.086
	AIC	28.861
	AICc	31.861
	BIC	30.699
	HQIC	26.193
Temkin	a_T (L mg^{-1})	7.573
	b_T	58.780
	R^2	0.929
	RSSE	580.929
	AIC	34.931
	AICc	37.931
	BIC	36.769
	HQIC	32.262
Dubinin−Radushkevich	Q_S (g mg^{-1})	139.920
	β (mol $kJ^{-1})^2$	1.350×10^{-7}
	E (kJ mol^{-1})	1.978
	R^2	0.989
	RSSE	87.449
	AIC	21.676
	AICc	24.676
	BIC	23.514
	HQIC	19.007

Table 4. Adsorption Capacities of AB-25 by Other Adsorbents as Compared with Cs−Trp@Fe_3O_4

adsorbent	adsorption capacity (mg/g)	reference
tarap peel	10.5	6
cempedak peel	21.2	
water lettuce	24.5	
CTAB−bentonite	22.5	20
base-treated Shorea dasyphylla	24.39	21
natural sepiolite	53.78	22
ahrimp shell	109.3	23
CHT−CGT film	151.5	24
CS−PVA@CuO	171.4	25
quaternized kenaf core fiber	303.03	26
Cs−Trp@Fe_3O_4	440.24	this study

$$\text{Removal efficiency (\%)} = 89.85 - 1.49x_i + 31.31x_{ii} + 2.86x_{iii} - 2.22x_ix_{ii} + 0.6042x_ix_{iii} - 2.26x_{ii}x_{iii} - 2.97x_i^2 - 21.31x_{ii}^2 + 0.2652x_{iii}^2 \quad (1)$$

https://doi.org/10.1021/acsomega.1c03964
ACS Omega 2021, 6, 30499−30514

Table 5. Experimental Design Matrix for the Adsorption of Acid Blue Dyes

	factors			removal efficiency (%)				
				actual values	predicted			
run	conc. (mg/L)	time (min)	dosage (g)	experimental	RSM	ANN	ANFIS	MLR
1	30.00	62.50	0.125	98.46	89.85	88.55	93.16	76.34
2	30.00	5.00	0.05	32.00	32.38	31.69	32.00	42.17
3	10.00	120.00	0.125	97.00	100.59	99.40	97.00	109.14
4	30.00	120.00	0.2	99.00	100.72	99.36	99.00	110.51
5	10.00	5.00	0.05	27.00	29.27	35.06	27.00	43.66
6	30.00	62.50	0.125	98.73	89.85	88.55	93.16	76.34
7	30.00	62.50	0.125	70.82	89.85	88.55	93.16	76.34
8	10.00	5.00	0.125	26.00	33.52	37.70	26.00	46.51
9	30.00	120.00	0.05	99.00	99.52	99.21	99.00	104.80
10	10.00	62.50	0.125	96.00	88.36	92.57	96.00	77.83
11	50.00	62.50	0.05	80.81	82.19	78.64	80.81	72.00
12	10.00	120.00	0.05	97.00	100.86	99.34	97.00	106.28
13	50.00	120.00	0.125	99.55	93.17	99.12	99.55	106.17
14	30.00	62.50	0.125	98.77	89.85	88.55	93.16	76.34
15	50.00	5.00	0.05	31.79	29.54	29.50	31.79	40.68
16	30.00	5.00	0.2	38.00	42.61	35.69	38.00	47.88
17	30.00	5.00	0.125	41.00	37.23	33.45	41.00	45.03
18	50.00	5.00	0.125	39.00	34.99	30.63	39.00	43.54
19	10.00	120.00	0.2	97.00	100.85	99.44	97.00	112.00
20	30.00	62.50	0.125	99.00	89.85	88.55	93.16	76.34
21	50.00	120.00	0.2	99.34	94.64	99.23	101.18	109.03
22	30.00	120.00	0.125	99.34	99.86	99.29	116.94	107.65
23	10.00	62.50	0.05	96.00	86.37	90.46	78.59	74.97
24	50.00	5.00	0.2	48.00	40.97	32.10	50.67	46.40
25	30.00	62.50	0.05	80.81	87.26	85.47	64.84	73.48
26	10.00	5.00	0.2	36.00	38.29	40.93	19.85	49.37
27	30.00	62.50	0.2	99.00	92.97	91.05	65.96	79.20
28	10.00	62.50	0.2	97.00	90.88	94.24	73.49	80.68
29	50.00	62.50	0.2	77.72	89.12	86.33	67.99	77.71
30	50.00	62.50	0.125	70.82	85.39	82.79	73.28	74.85
31	50.00	120.00	0.05	95.21	92.23	98.98	109.85	103.31
32	30.00	62.50	0.125	77.72	89.85	88.55	93.16	76.34

The significance of these quadratic models was estimated using analysis of variance (ANOVA) based on the values of F-test and related p-values. The coefficients of determination (R^2 and adj. R^2) were used to compare the experimental and predicted results. The optimum operating conditions were determined from the fitting parameters obtained for independent variables.

The ANOVA results of the model presented in Table 6 showed that the removal efficiency of the AB-25 dye by Cs−Tp@Fe_3O_4 displayed F values that indicate significant results. The relationship between variables and the target can be explained by the model with a deviation less than 0.2. The p-values < 0.05, as well as the high sum of squares obtained for the dye removal, implies the significance of the variables and a proof that the model regression is significant.[27,28] The degree of precision (% CV) of 11.61% confirmed some high precision and reliability of the model, while the adequate precision value of 14.46 shows that the model is desirable and possesses adequate signal to navigate the design space. Also, the R^2 indicates that 92.67% of variability can be accounted for by the model. Based on the p-values at 95% confidence limit ($p < 0.005$), we can say that the contact time played a significant role in the dye removal efficiency. Upon removal of insignificant factors, as shown in the ANOVA, eq 1 can be written as

$$\text{removal efficiency (\%)} = 89.85 + 31.31 \times \text{time} - 21.31 \times \text{time}^2 \quad (1b)$$

The interactions of the coefficients of these variables as well as those of their quadratics except that of contact time are insignificant. The F-values were large enough to describe the developed models significantly. The overall rating based on the insignificant lack of fit from ANOVA implied that the model is significant.

Figure 6a−c displays the response surface plots of the variation of the dye removal efficiency with the initial dye concentration, contact time, and adsorbent dosage obtained from the polynomial models of eq 1. It can be seen from the figures that the interaction of the independent variables has an effect on the removal efficiency. The general trend is an increase in the efficiency as these variable increases up to an optimum point where a further increase has no significant effect on the removal efficiency. The main effect model showed that the contact time and the interactions of the initial concentration and the adsorbent dosage positively influenced the removal efficiency of the AB-25 dye by Cs−Trp@Fe_3O_4. The numerical optimization analysis on Design Expert software, showed that the maximum removal efficiencies of over 100% is feasible under the optimum conditions of an initial concentration of 22.10 mg/

https://doi.org/10.1021/acsomega.1c03964
ACS Omega 2021, 6, 30499−30514

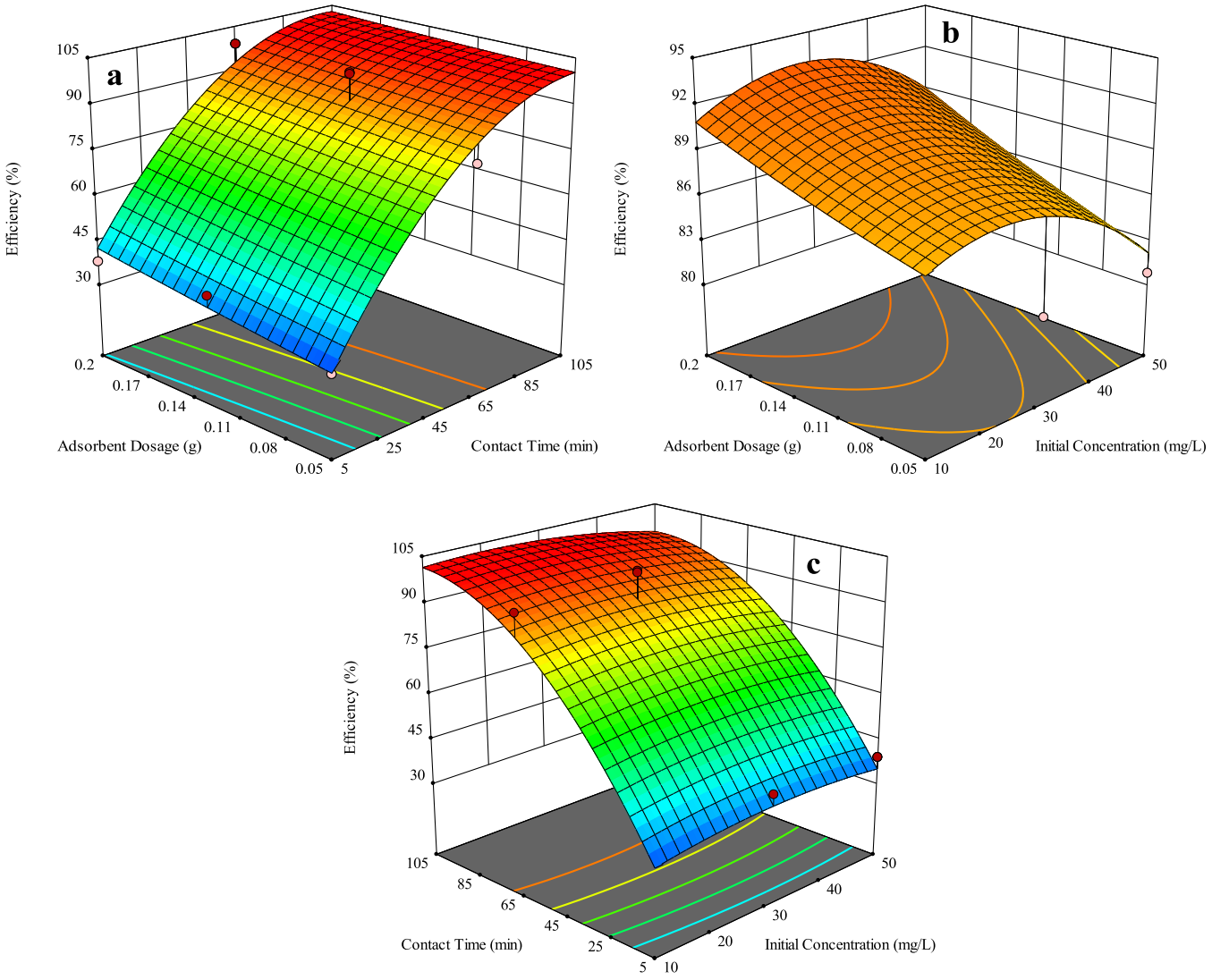

Figure 6. Response surface plot of the effect of (a) adsorbent dosage and contact time, (b) adsorbent dosage and initial concentration, and (c) contact time and adorbent dosage on the removal efficiencies of the AB-25 dye by Cs−Trp@Fe_3O_4.

Table 6. ANOVA Results for the Removal Efficiency

source	sum of squares	DF	mean square	*F*-value	*p*-value	
model	21821.65	9	2424.63	30.89	<0.0001	significant
x_i—conc (mg/L)	39.78	1	39.78	0.5069	0.4840	
x_{ii}—time (min)	17650.07	1	17650.07	224.88	<0.0001	significant
x_{iii}—dosage (g)	147.00	1	147.00	1.87	0.1850	
$x_i\, x_{ii}$	59.36	1	59.36	0.7563	0.3939	
$x_i\, x_{iii}$	4.38	1	4.38	0.0558	0.8154	
$x_{ii}\, x_{iii}$	61.11	1	61.11	0.7786	0.3871	
x_i^2	63.31	1	63.31	0.8066	0.3788	
x_{ii}^2	3248.63	1	3248.63	41.39	<0.0001	significant
x_{iii}^2	0.5030	1	0.5030	0.0064	0.9369	
residual	1726.74	22	78.49			
lack of fit	904.41	17	53.20	0.3235	0.9636	not significant
pure error	822.33	5	164.47			
cor total	23548.39	31				
R^2	0.9267					
adjusted R^2	0.8967					
predicted R^2	0.8694					
adeq precision	14.46					
% CV	11.61					

https://doi.org/10.1021/acsomega.1c03964
ACS Omega 2021, 6, 30499−30514

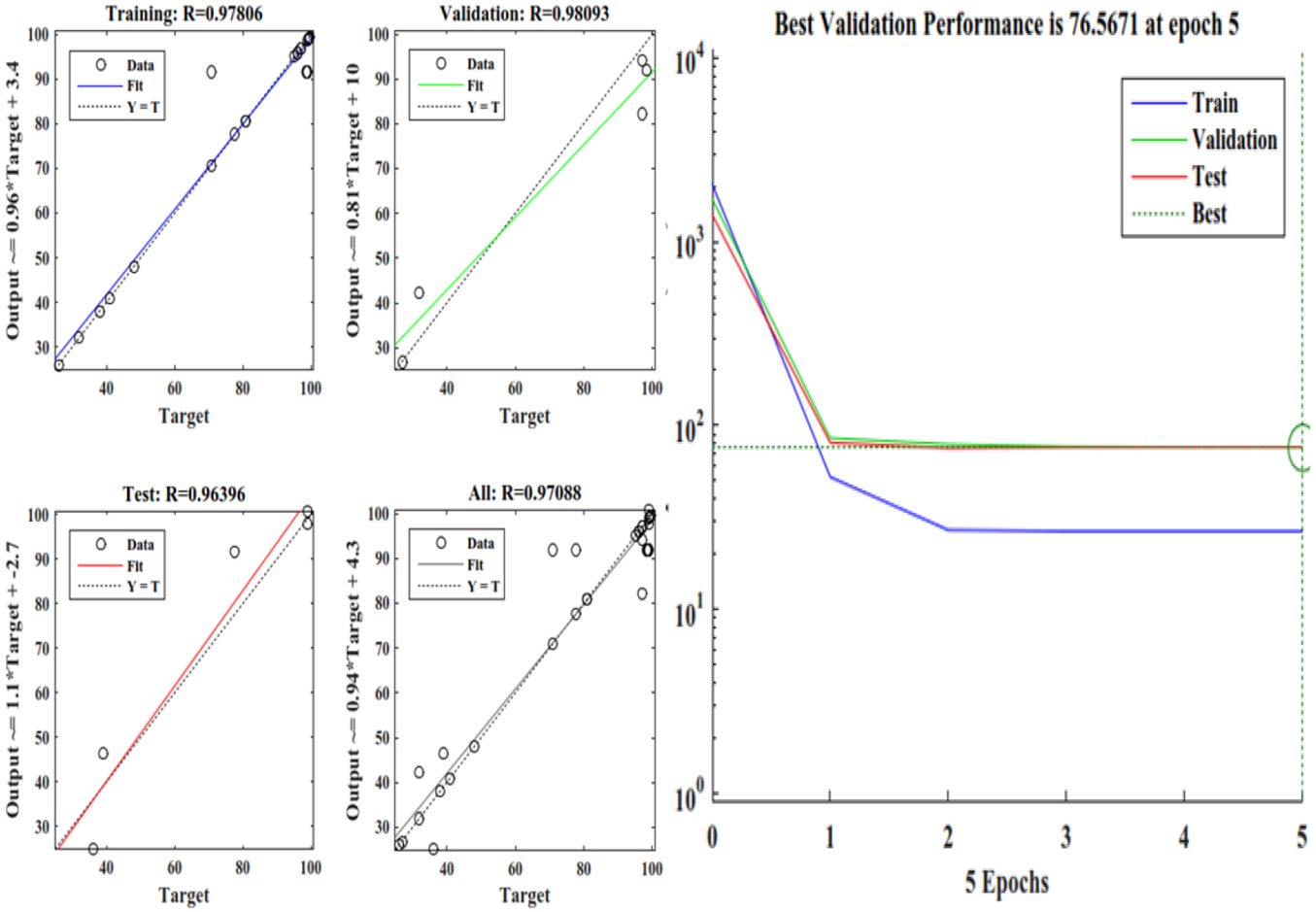

Figure 7. ANN training and performance.

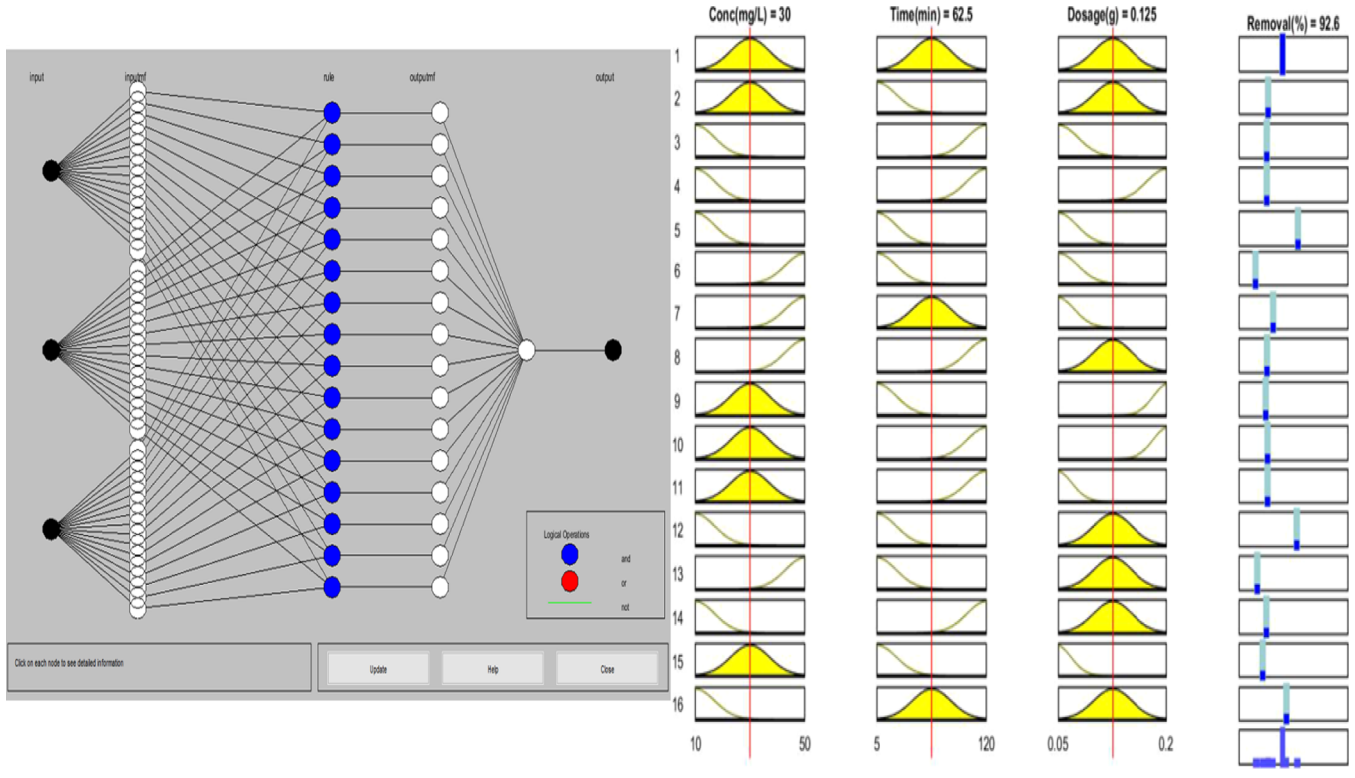

Figure 8. Proposed ANFIS structure and its performance.

https://doi.org/10.1021/acsomega.1c03964
ACS Omega 2021, 6, 30499−30514

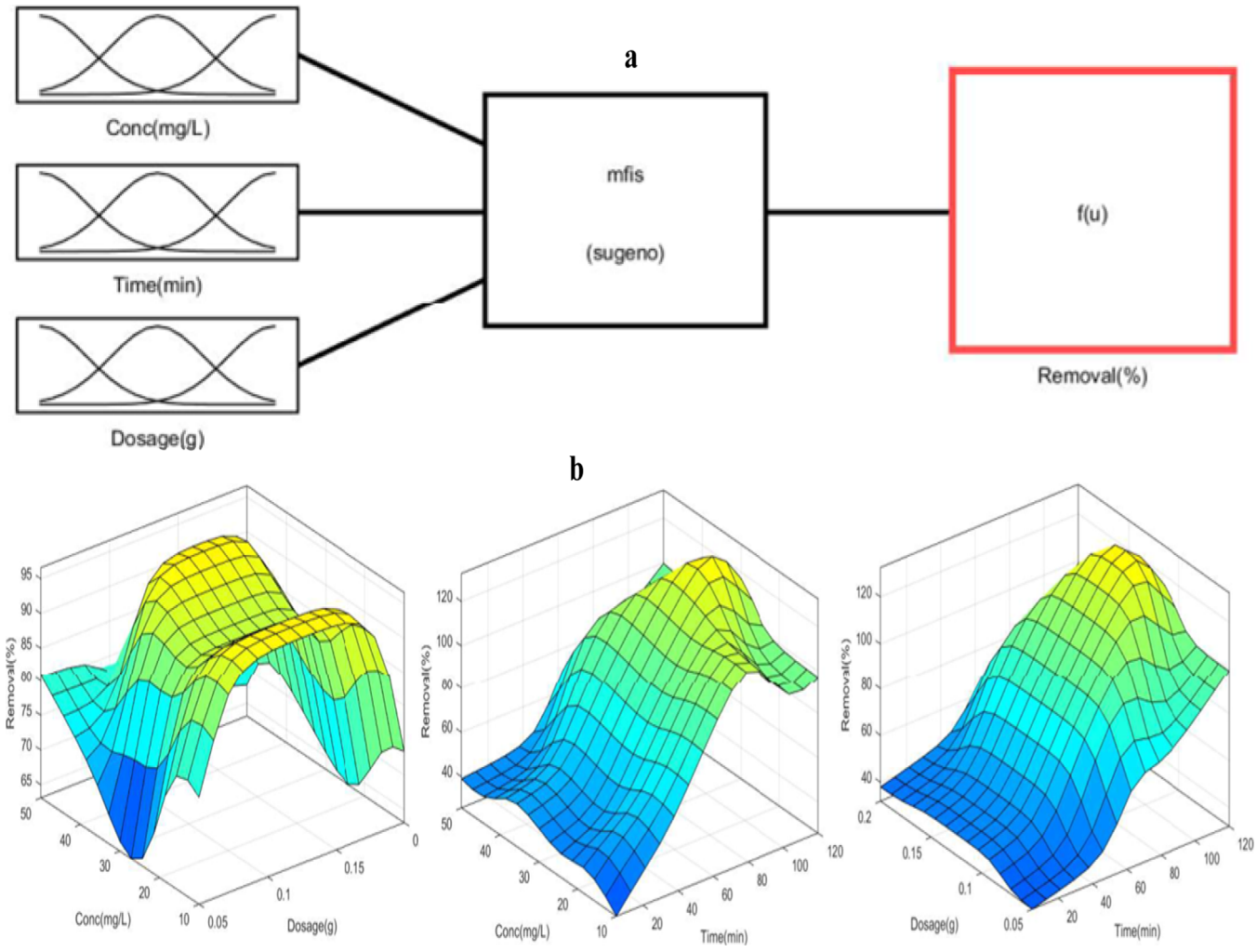

Figure 9. (a) Sugeno-type FIS and (b) 3D plots predicted by ANFIS.

L, a contact time of 104.2 min, and an adsorbent dosage of 0.186 g.

ANN Analysis. Data in Table 5 were subjected to ANN analysis; the 32 experimental data sets with the initial dye concentration, contact time, and adsorbent dosage were taken as the input variables, while the removal efficiency of AB-25 was considered the target variable. The ANN modeling was performed by feeding the data set into the ANN architecture, 20 (60%) data sets were used for algorithm training, while 6 (20%) data sets each were used for the validation and testing. The Levenberg−Marquardt algorithm was selected as the training algorithm, and the number of hidden neurons was increased from 10 to 14 with a decrease in the mean square error (MSE) from 6300 to 76.56 after which there was no significant change in the MSE values. The best training performance was obtained after six iterations and five epochs, and the details of training and performance are shown in Figure 7.

ANFIS Analysis. Data in Table 5 were subjected to ANFIS analysis using the ANFIS Editor user interface in the Fuzzy Logic Toolbox of MATLAB for ANFIS modeling and simulation. The grid partition and subtractive clustering methods were used to generate the optimized sets of rules. A hybrid algorithm was used for the training of the FIS, while the model accuracy was tested with testing and validation data sets; Figure 8 shows the proposed ANFIS structure and its performance, the optimum of which predicted a 92.8% removal at an initial concentration of 50 mg/L, a contact time of 62.5 min, and an adsorbent dosage of 0.125, in agreement with the experimental observation. In order to verify the prediction performance of the proposed ANFIS model, the predicted removal efficiency values were determined in different ways. The ANFIS model was trained and tested with the training and testing data sets, and the Sugeno-type FIS generated for training ANFIS, as shown in Figure 9a, has a combination of inputs, with the output of the ANFIS having minima and maxima values. 3D plots for the predicted removal efficiency using the ANFIS model are shown in Figure 9b with a clear demonstration of nonlinear behavior of the process.

Multiple Linear Regression Analysis. Multiple linear regression (MLR) was used to predict the effects of the experimental variables on the efficiency of the adsorbent for AB-25 dye removal; the equation of regression relating the efficiency with the variables is given as

$$\text{removal efficiency (\%)} = 39.7705 - 0.7433 \times \text{conc} + 0.5446 \times \text{time} + 38.1037 \times \text{dosage} \quad (2)$$

https://doi.org/10.1021/acsomega.1c03964
ACS Omega 2021, 6, 30499−30514

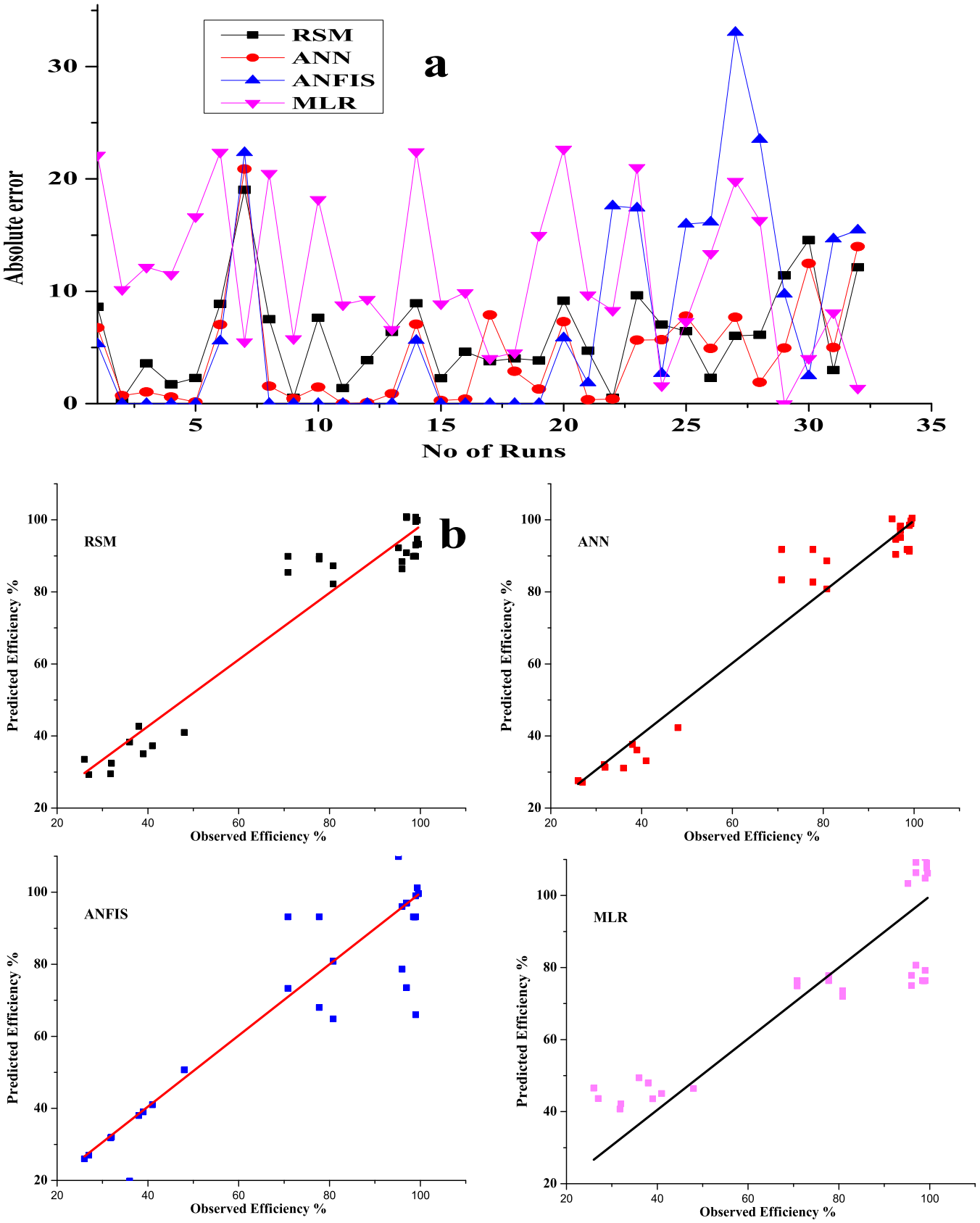

Figure 10. (a) Plots of the absolute errors and (b) models' comparison.

Based on the determination coefficient (R^2 = 75.75%) obtained from the fit, the total variation out of the scope of the model is estimated as 24.25% (residuals).

Comparison of RSM, ANN, ANFIS, and MLR. Deviations of the modeled values from the observed values of removal efficiency can easily be demonstrated by the plot of the absolute

https://doi.org/10.1021/acsomega.1c03964
ACS Omega 2021, 6, 30499−30514

errors of the models determined and observed values, as shown in Figure 10a. The deviation interval of the predicted values from the model are in the order of ANFIS > MLR > ANN > RSM with ranges between 0.0 and 33.04, 0.0 and 22.65, 0.0 and 20.88, and 0.38 and 19.03, respectively. Similarly, the correlation between the models was tested, as shown graphically in Figure 10b. A good fit between the model results and experimental results is obvious in RSM and ANN. MLR, the accuracy, and the predictive ability of the models are in the order of RSM > ANN > ANFIS > MLR, as shown by the values of MSE, root-mean-square error (RMSE), sum square error (SSE), mean absolute error (MAE), and R^2 in Table 7. The lower values of R^2 in the MLR model resulted in a greater deviation in fitting to the measured responses than those of other models, although its RMSE value compared favourably with that of the ANFIS. Thus, it can be inferred that RSM and ANN best modeled the adsorption process under the conditions of investigation (Table 8).

Table 7. Fitting Parameters for the Models

	MSE	RMSE	SSE	MAE	R^2
RSM	49.347	7.304	33.975	6.006	0.927
ANN	37.920	6.643	24.652	4.358	0.946
ANFIS	113.167	11.259	38.031	6.723	0.850
MLR	163.186	12.009	65.072	11.503	0.757

Table 8. Central Composite Design

			range and level of factors		
variable	unit	factor code/ notation	−1	0	+1
initial dye conc.	mg/L	x_i	10	30	50
contact time	Min	x_{ii}	5	62.5	120
adsorbent dosage	G	x_{iii}	0.05	0.125	0.2

CONCLUSIONS

Cs−Tp@Fe_3O_4 was successfully synthesized and confirmed by characterization. The as-synthesized adsorbent was used for the removal of AB-25 from aqueous solutions. The effects of interactions of dye concentrations, contact time, and adsorbent dosage were modeled using RSM, ANN, ANFIS, and MLIR. The data obtained from time-dependent adsorption showed that first-order kinetics best model the process, and that the mechanism is not solely on diffusion control. All the adsorption isotherms investigated modeled the isotherm satisfactorily in the order of Dubinin−Radushkevich > Langmuir > Freundlich > Temkin based on the R^2 values. The RSM model with a R^2 value of 0.927 is an indication that the obtained model is significant and can optimize the experimental conditions successfully. The accuracy and the predictive ability of the models are in the order of RSM > ANN > ANFIS > MLR based on the R^2 value. The high adsorption capacity obtained for the synthesized adsorbent puts it at an advantage over other adsorbents for the removal of AB-25 compared to other adsorbents in the same category.

MATERIALS AND METHODS

Materials. The following materials were used: acid blue 25 (AB-25), a sodium salt of 1-amino-4-anilino-9,10-dioxo-9,10-dihydroanthracene-2-sulfonate (C.I. no. 62055), chitosan powder of molecular weight 100,000−300,000, and terephthalic acid ($C_6H_4(CO_2H)_2$) from Acros Organics; glutaraldehyde from Alfa Aesar; ferrous chloride tetrahydrate ($FeCl_2{\cdot}4H_2O$) and ferric chloride hexahydrate ($FeCl_3{\cdot}6H_2O$) from Sigma Aldrich; and NH_4OH and NaOH from Merck, India; other chemicals used were of Analar grade, and double distilled water was used for all of the experiments.

Synthesis of Cs−Tp@Fe_3O_4 Nanoparticles. Cs−Tp@Fe_3O_4 nanoparticles were synthesized in two stages. 2.70 g of $FeCl_3{\cdot}6H_2O$, 0.994 g of $FeCl_2{\cdot}4H_2O$, and 1.66 g of $C_6H_4(CO_2H)_2$ were introduced into a round-bottom flask containing 50 mL of double distilled deionized water and heated gradually under continuous stirring until the temperature reached 70 °C. After 1 h of continuous stirring/heating, 30 mL of 35% liquid ammonia was added dropwise with stirring, and the temperature was further maintained for another 1 h. The black nanoparticles obtained were washed with deionized water and ethanol three times and dried under vacuum at 60 °C for 12 h.

A solution of chitosan was prepared by activating 1.0 g of powder in 50 mL of 1% glacial acetic acid solution and stirred at 80 °C for 4 h. Synthesis of Cs−Tp@Fe_3O_4 was accomplished in the second step by adding the chitosan solution gradually to the dispersed mixture of the previously prepared nanoparticles under continuous stirring at 80 °C for 2 h. Beads were prepared by dropping the resulting mixture into a stirred 1 M NaOH solution using a narrow tube controlled by a peristaltic pump. The beads were left overnight in the basic solution and then filtered.

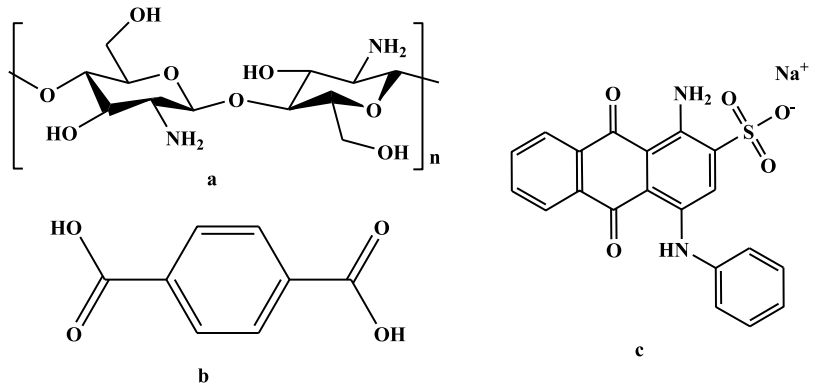

Figure 11. Structures of (a) chitosan (b) terephthalic acid, and (C) AB-25 dye.

https://doi.org/10.1021/acsomega.1c03964
ACS Omega 2021, 6, 30499−30514

About 20.0 g of wet beads were soaked in 25 mL of 1% glutaraldehyde and left for 24 h to allow for crosslinking. The beads were then filtered off. The beads were then washed with distilled water until the filtrate had a pH of 7, rinsed with acetone, followed by drying in a vacuum oven at 80 °C for 12 h.

Characterization of the Synthesized Cs−Tp@Fe_3O_4 Nanoparticles. The surface morphology and elemental composition of the obtained material were analyzed using a scanning electron microscope Carl Zeiss EVO 15 equipped with an Oxford INCA 350 EDX system; XRD data were collected on a Bruker XRD D2 PHASER 2θ/scan Cu tube with a LYNXEYE (ID mode) detector run from 10 to 80 2θ and resolved on DIFFRAC.SUITE EVA software (VERSION 4.2.1.10) (λ = 1.5418 Å). The IR spectra were collected on a Bruker ATR-FTIR spectrometer at a resolution of 4 cm^{-1} and recorded from 400 to 4000 cm^{-1}. UV−visible measurements were carried out on an Evolution 220 UV−vis spectrophotometer, Thermo Scientific and analyzed with Thermo Scientific INSIGHT 2 software (version 2.3.345). The results obtained were compared among chitosan, Tp@Fe_3O_4, and Cs−Tp@Fe_3O_4.

Adsorption Studies. A stock solution of AB-25 dye was prepared by dissolving an accurately weighed solute such that the solution contained 1 g equiv of the dyes (Figure 11) in 1 L distilled water, and working standard solutions were then prepared from the stock by dilution. The pH of the working solution was maintained with an aliquot of HCl or NaOH prior to the adsorption study.

The batch equilibrium and adsorption kinetics studies were conducted in a batch process in glass flasks, each containing 25 mL of dye solution with concentrations ranging between 10 and 50 mg/L and 0.1 g of the adsorbent. The contents were placed in a regulated water bath (30 ± 1 °C) with a shaker and shaken at 150 rpm. Samples of the aqueous phase were withdrawn at preset time intervals (0−240 min), and the dye concentration was determined using a UV−vis spectrophotometer. The amounts of dye adsorbed (mg/g) by the adsorbents as a function of time (Q_t) and at equilibrium (Q_e) were determined according to eqs 3 and 4, respectively

$$Q_t = \frac{(C_o - C_t) \times V}{m} \tag{3}$$

$$Q_e = \frac{(C_o - C_e) \times V}{m} \tag{4}$$

where C_o, C_t, and C_e are the initial, time t, and equilibrium concentrations (mg L^{-1}) of the dye, respectively; V is the volume (L) of the solution; and m is the mass (g) of the adsorbent.

Kinetics and Equilibrium Data Modeling. *Adsorption Mechanism.* The mechanism of adsorption of the dye onto Cs−Tp@Fe_2O_3 was investigated from the kinetic data by modeling the data with Lagergren's pseudo-first order, Ho's pseudo-second order, Elovich, and Weber−Morris intra-particle diffusion models (eqs 4−7, respectively).[28,29]

$$Q_t = Q_e(1 - e^{-k_1 t}) \tag{5}$$

$$Q_t = \frac{k_2 Q_e^{\,2} t}{1 + k_2 Q_e t} \tag{6}$$

$$Q_t = \frac{1}{\beta_E} \ln(\alpha_E \beta_E t) \tag{7}$$

$$Q_t = k_{id} t^{1/2} + C \tag{8}$$

Adsorption Isotherms. Adsorption equilibrium is established when an adsorbate-containing phase was in contact with the adsorbent for a sufficient time period, so that the adsorbate concentration in the bulk solution is in dynamic equilibrium with the interface concentration.[30] Thus, data obtained from the equilibrium adsorption were subjected to the Langmuir, Freundlich, Temkin, and Dubinin−Radushkevich isotherm models, as described in eqs 8−11, respectively. These models described the phenomenon governing the retention, release, or mobility of a substance from the aqueous porous media or aquatic environments to a solid phase at constant temperature and pH.[28,31]

$$Q_e = \frac{Q_0 K_L C_e}{1 + K_L C_e} \tag{9}$$

$$Q_e = K_F C_e^{\,1/n} \tag{10}$$

$$Q_e = \frac{R_g T}{b_T} \ln a_T C_e \tag{11}$$

$$Q_e = Q_m e^{-\beta \varepsilon^2} \tag{12}$$

Model Selection. The coefficient of determination (R^2) had been extensively used for comparing and selecting the best model fits for adsorption kinetics and isotherm studies; however, this approach does not take into consideration the number of parameters in a model and thus is perpetually in favor of higher parameter models. Therefore, it has been adjudged as a poor method for model selection.[32] Methods that account for a model's goodness-of-fit based on the number of parameters are better suited for model selection; these include IC and likelihood ratio tests (LRT). Model selection based on IC is advantageous owing to the ease of interpretation and the fact that it can be used to compare both nested and non-nested models. The models are ranked and the "best model" is the one with the lowest or most negative IC when comparing models fitted to the same data. This study will exploit AIC, BIC, as well as HQIC, details of which can be found in literature.[33,34] These are employed not only for the best model selection but also for the ranking of the kinetics and isotherm models deployed in this study.

Statistical Analysis. *Design of Experiments and Statistical Analysis.* The influence of the contact time, initial dye concentration, and adsorbent dosage and the interactions of the factors and the adsorption of AB-25 dye by Cs−Tp@Fe_3O_4 were investigated using the FCC design of experiments. Start-Ease Design Expert software (version 11.1.2.0) was deployed for the design, and the factors' ranges were selected after a series of preliminary experiments. Regression and other statistical analyses of the factors' range of initial dye concentration (10−50 mg/L), contact time (5−120 min), and adsorbent dosage (0.05−0.2 g) are presented according to Table 1:

The experimental data obtained were subjected to the second-order polynomial regression model. The response Y which represents the removal efficiencies (% dye removal) can be related to the independent variables as a polynomial model based on the quadratic equation in eq 13, where z_0, z_i, z_{ii}, *and* z_{ij} are the regression coefficient of the intercept, the linearity, the square, and the interaction terms respectively, while x_i, x_{ii}, and x_j are the independent variables.

https://doi.org/10.1021/acsomega.1c03964
ACS Omega 2021, 6, 30499−30514

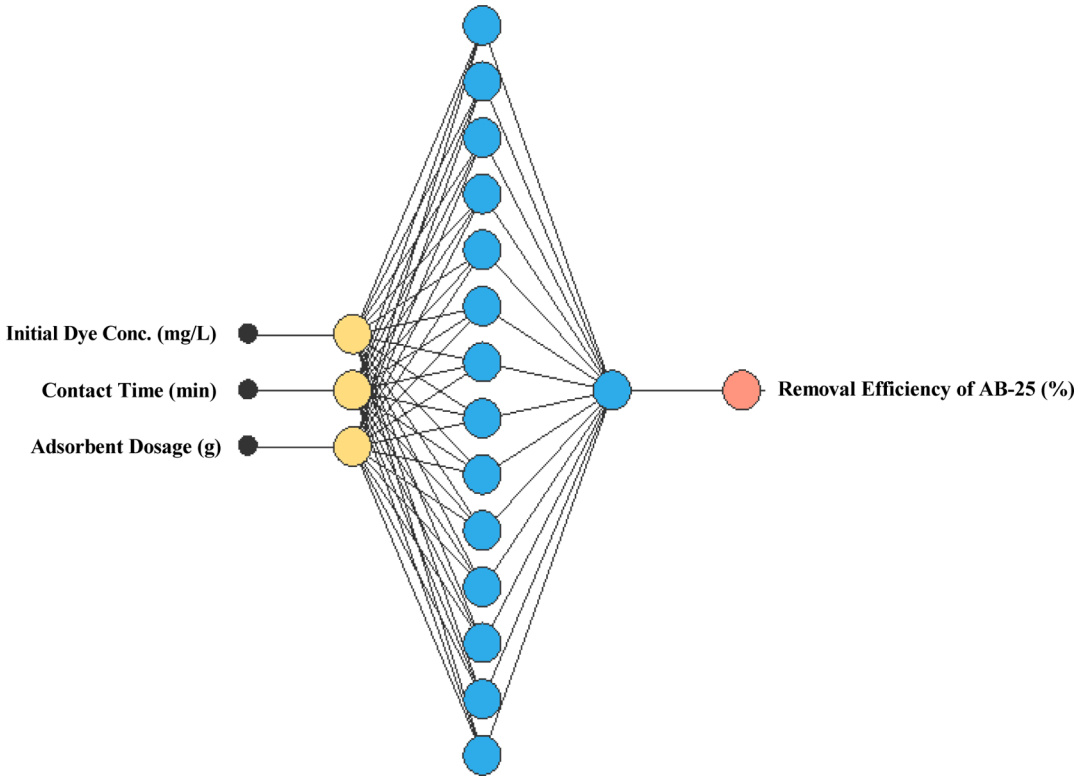

Figure 12. ANN architecture.

$$Y = z_0 + \sum_{i=1}^{n} z_i x_i + \sum_{i}^{i<j} \sum_{j} z_{ij} x_i x_j + \sum_{i=1}^{n} z_{ii} {x_i}^2 \quad (13)$$

The analysis of variance (ANOVA) was employed to evaluate the adequacy of the developed model and the statistical significance of the regression coefficients, as well as the evaluation of the individual, interactive, and quadratic effects of the process variables on the removal efficiency of AB-25 using Cs−Tp@Fe_3O_4 nanoparticles. The model terms were assessed using the *p*-value with a confidence level of 95%. Fisher's *F*-value was used to examine the significance of the regression coefficients. In addition, the coefficient of determination (R^2) value was compared to the adjusted R^2 value to check the adequacy of the model. Three-dimensional surface and contour plots of the independent variables' interactive effects with their corresponding responses were obtained to observe the interaction between the process variables and their corresponding effect on the output response.

A three-layer (input−hidden−output) computational neural network was used in this study as it has been demonstrated that this kind of ANN using sigmoid transfer functions can easily map any function of practical interest.[35] The input layers contain three nodes, each for the independent variable with an output layer generating the scaled estimated values for the removal efficiencies of AB-25 dye. The training algorithm with 14 hidden layer neuron architecture was adopted for the study. Figure 12 depicts the 3:14:1 ANN architecture used for the analysis. Levenberg−Marquardt based on MATLAB function "TRAINLM" at the hidden layer and the linear transfer function "PURLIN" at the output were selected for modeling the adsorption removal of AB-25 dye by Cs−Tp@Fe_3O_4.

The hyperbolic tangent "TANSIG" (eq 14) was selected for the input to hidden layer mapping, while the hidden layer to the output layer mapping was obtained from a purely linear transfer function "PURELIN"(eq 15).[28] Several training runs were performed for the best possible weights in the error back-propagation framework.

$$\hat{y} = \tan \text{sig}\,(u) = \frac{2}{(1 + e^{-2u}) - 1} \quad (14)$$

$$\%\ \text{removal} = w \times Y + b \quad (15)$$

The normalized input, predicted normalized output data, and predicted renormalized data are denoted u, $\hat{y}$, and Y, respectively, while the ANN parameters' weights and biases are denoted w and b, respectively.

ANFIS is an artificial intelligence system that proffers an alternative to the polynomial regression method as a modeling tool. It is a flexible means of analysis with respect to the number and form of the experimental data, thus making the possibility of utilization of experimental designs rather than statistical approaches. The ANFIS used in this study possesses a feed-forward neural network structure where each layer is a neuro-fuzzy system component developed by Roger Jang in 1993.[36]

An MLR model was used to model the impacts of numerous independent variables on the dependent variable. The MLR model can be expressed by the mathematical equation as

$$y = \beta_0 + \sum_{i=1}^{n} \beta_i x_i + \varepsilon \quad (16)$$

where y is the predicted value by the MLR model, β_i $(i = 1,...,n)$ and x_i $(i = 1,...,n)$ are the partial regression coefficients and the independent variables (inputs), respectively, while ε is a random or an unexplained error.[37−39]

In this study, the performance of the RSM, ANN ANFIS, and MLR models was statically evaluated by the MSE, RMSE, MAE,

https://doi.org/10.1021/acsomega.1c03964
ACS Omega 2021, 6, 30499−30514

SSE, and R^2. The MATLAB R2015a (The Mathworks, Inc. ver. 8.5.0) computing environments of the neural network toolbox, ANFIS editor, and stepwise analysis were used to generate the ANN, ANFIS, and MLR models from the data.

AUTHOR INFORMATION

Corresponding Author

Abideen Idowu Adeogun − *Chemistry Department, Federal University of Agriculture, Abeokuta 110001, Nigeria;* orcid.org/0000-0003-2587-9261; Phone: +2348036126987; Email: adeogunai@funaab.edu.ng; Fax: +2348036126987

Authors

Caroline Avosuahi Akinremi − *Chemistry Department, Federal University of Agriculture, Abeokuta 110001, Nigeria; Faculty of Health and Life Sciences, De Montfort University, Leicester LE1 9BH, U.K.*

Maxime Poupin − *Centre Universitaire de la Charente, Université de Poitiers, La Couronne 16400, France*

Katherine Huddersman − *Faculty of Health and Life Sciences, De Montfort University, Leicester LE1 9BH, U.K.*

Complete contact information is available at: https://pubs.acs.org/10.1021/acsomega.1c03964

Notes

The authors declare no competing financial interest.

ACKNOWLEDGMENTS

The authors acknowledge the research grant provided by Schlumberger Faculty for the Future Fellowship for Dr. Caroline Akinremi utilized at De Montfort University, Leicester, UK. The authors also wish to thank the Federal University of Agriculture FUNAAB for their encouragement.

REFERENCES

(1) Norton, B. Industrial and Agricultural Applications of Solar Heat. *Comprehensive Renewable Energy*; Ali, S., Ed; Elsevier, 2012; pp 567−594.

(2) Ben Mansour, H.; Corroler, D.; Barillier, D.; Ghedira, K.; Chekir, L.; Mosrati, R. Evaluation of genotoxicity and pro-oxidant effect of the azo dyes: acids yellow 17, violet 7 and orange 52, and of their degradation products by Pseudomonas putida mt-2. *Food Chem. Toxicol.* **2007**, *45*, 1670−1677.

(3) Bello, O. S.; Adegoke, K. A.; Sarumi, O. O.; Lameed, O. S. Functionalized locust bean pod (Parkiabiglobosa) activated carbon for Rhodamine B dye removal. *Heliyon* **2019**, *5*, No. e02323.

(4) Ofudje, E. A.; Adeogun, I. A.; Idowu, M. A.; Kareem, S. O.; Ndukwe, N. A. Simultaneous removals of cadmium (II) ions and reactive yellow 4 dye from aqueous solution by bone meal-derived apatite: kinetics, equilibrium and thermodynamic evaluations. *Anal. Sci. Technol.* **2020**, *11*, 7.

(5) Yaseen, D. A.; Scholz, M. Textile dye wastewater characteristics and constituents of synthetic effluents: a critical review. *Int. J. Environ. Sci. Technol.* **2019**, *16*, 1193−1226.

(6) Kooh, M. R. R.; Dahri, M. K.; Lim, L. B.; Lim, L. H.; Chan, C. M. Separation of acid blue 25 from aqueous solution using water lettuce and agro-wastes by batch adsorption studies. *Appl. Water Sci.* **2018**, *8*, 61.

(7) National Center for Biotechnology Information. PubChem Compound Summary for CID 23675622, Acid Blue 25. 2021. Retrieved August 18, 2021 from https://pubchem.ncbi.nlm.nih.gov/compound/Acid-Blue-25

(8) Adeogun, A. I.; Osideko, O. A.; Idowu, M. A.; Akinloye, O. A.; Ofudje, E. A. Synthesis, characterization and investigation of chitosan-functionalized ZnFe2O4 for the removal of dichlorvos from aqueous solution. *J. Dispersion Sci. Technol.* **2021**, 1−10.

(9) Hu, B.; Wang, K.; Wu, L.; Yu, S.-H.; Antonietti, M.; Titirici, M.-M. Engineering carbon materials from the hydrothermal carbonization process of biomass. *Adv. Mater.* **2010**, *22*, 813−828.

(10) Xie, P.; Li, H.; He, B.; Dang, F.; Lin, J.; Fan, R.; Hou, C.; Liu, H.; Zhang, J.; Ma, Y.; Guo, Z. Bio-gel derived nickel/carbon nanocomposites with enhanced microwave absorption. *J. Mater. Chem. C* **2018**, *6*, 8812−8822.

(11) Xie, X.; Hu, Y.; Cheng, H. Rapid degradation of p-arsanilic acid with simultaneous arsenic removal from aqueous solution using Fenton process. *Water Res.* **2016**, *89*, 59−67.

(12) Tanhaei, B.; Ayati, A.; Iakovleva, E.; Sillanpää, M. Efficient carbon interlayed magnetic chitosan adsorbent for anionic dye removal: Synthesis, characterization and adsorption study. *Int. J. Biol. Macromol.* **2020**, *164*, 3621−3631.

(13) Shajahan, A.; Shankar, S.; Sathiyaseelan, A.; Narayan, K. S.; Narayanan, V.; Kaviyarasan, V.; Ignacimuthu, S. Comparative studies of chitosan and its nanoparticles for the adsorption efficiency of various dyes. *Int. J. Biol. Macromol.* **2017**, *104*, 1449−1458.

(14) Alves, N. M.; Mano, J. F. Chitosan derivatives obtained by chemical modifications for biomedical and environmental applications. *Int. J. Biol. Macromol.* **2008**, *43*, 401−414.

(15) da Silva Alves, D. C.; Healy, B.; Pinto, L. A. d. A.; Cadaval, T. R. S. A.; Breslin, C. B. Recent Developments in Chitosan-Based Adsorbents for the Removal of Pollutants from Aqueous Environments. *Molecules* **2021**, *26*, 594.

(16) Nguyen, V. C.; Pho, Q. H. Preparation of chitosan coated magnetic hydroxyapatite nanoparticles and application for adsorption of reactive blue 19 and Ni2+ ions. *Sci. World J.* **2014**, *2014*, 273082.

(17) Akinremi, C. A.; Oyelude, V. B.; Adewuyi, S.; Amolegbe, S. A.; Arowolo, T. Reduction of Bromate in Water using Zerovalent Cobalt 2,6-Pyridine Dicarboxylic Acid Crosslinked Chitosan Nanocomposite. *J. Macromol. Sci., Part A: Pure Appl. Chem.* **2013**, *50*, 435−440.

(18) Adeogun, A. I.; Akande, J. A.; Idowu, M. A.; Kareem, S. O. Magnetic tuned sorghum husk biosorbent for effective removal of cationic dyes from aqueous solution: isotherm, kinetics, thermodynamics and optimization studies. *Appl. Water Sci.* **2019**, *9*, 160.

(19) Zhou, X.; Zhou, X. The unit problem in the thermodynamic calculation of adsorption using the Langmuir equation. *Chem. Eng. Commun.* **2014**, *201*, 1459−1467.

(20) Jeeva, M.; Wan Zuhairi, W. Y. Adsorption of Acid Blue 25 dye by bentonite and surfactant modified bentonite. *AIP Conf. Proc.* **2018**, *1940*, 020030 No. 1.

(21) Hanafiah, M. A. K. M.; Ngah, W. S. W.; Zolkafly, S. H.; Teong, L. C.; Majid, Z. A. A. Acid Blue 25 adsorption on base treated Shoreadasyphylla sawdust: Kinetic, isotherm, thermodynamic and spectroscopic analysis. *J. Environ. Sci.* **2012**, *24*, 261−268.

(22) Han, Z.-X.; Zhu, Z.; Wu, D.-D.; Wu, J.; Liu, Y.-R. Adsorption kinetics and thermodynamics of acid blue 25 and methylene blue dye solutions on natural sepiolite. *Synth. React. Inorg., Met.-Org., Nano-Met. Chem.* **2014**, *44*, 140−147.

(23) Daneshvar, E.; Sohrabi, M. S.; Kousha, M.; Bhatnagar, A.; Aliakbarian, B.; Converti, A.; Norrström, A.-C. Shrimp shell as an efficient bioadsorbent for Acid Blue 25 dye removal from aqueous solution. *J. Taiwan Inst. Chem. Eng.* **2014**, *45*, 2926−2934.

(24) Haque, A. N. M. A.; Remadevi, R.; Wang, X.; et al. Adsorption of anionic Acid Blue 25 on chitosan-modified cotton gin trash film. *Cellulose* **2020**, *27*, 9437−9456.

(25) Lakkaboyana, S. K.; Soontarapa, K.; Vinaykumar, R. K.; Marella, R. K.; Kannan, K. Preparation of novel chitosan polymeric nanocomposite as an efficient material for the removal of Acid Blue 25 from aqueous environment. *Int. J. Biol. Macromol.* **2021**, *168*, 760−768.

(26) Idan, I. J.; Abdullah, L. C.; Choong, T. S.; Jamil, S. N. A. B. M. Equilibrium, kinetics and thermodynamic adsorption studies of acid dyes on adsorbent developed from kenaf core fiber. *Adsorpt. Sci. Technol.* **2018**, *36*, 694−712.

(27) Guvenc, S. Y.; Erkan, H. S.; Varank, G.; Bilgili, M. S.; Engin, G. O. Optimization of paper mill industry wastewater treatment by

https://doi.org/10.1021/acsomega.1c03964
ACS Omega 2021, 6, 30499−30514

electrocoagulation and electro-Fenton processes using response surface methodology. *Water Sci. Technol.* **2017**, *76*, 2015−2031.
(28) Adeogun, A. I.; Bhagawati, P. B.; Shivayogimath, C. B. Pollutants removals and energy consumption in electrochemical cell for pulping processes wastewater treatment: Artificial neural network, response surface methodology and kinetic studies. *J. Environ. Manage.* **2021**, *281*, 111897.
(29) Vahidhabanu, S.; Abideen Idowu, A.; Karuppasamy, D.; Ramesh Babu, B.; Vineetha, M. Microwave initiated facile formation of sepiolite-poly (dimethylsiloxane) nanohybrid for effective removal of congo red dye from aqueous solution. *ACS Sustainable Chem. Eng.* **2017**, *5*, 10361−10370.
(30) Kumar, A.; Kumar, S.; Kumar, S.; Gupta, D. V. Adsorption of phenol and 4-nitrophenol on granular activated carbon in basal salt medium: equilibrium and kinetics. *J. Hazard. Mater.* **2007**, *147*, 155−166.
(31) Limousin, G.; Gaudet, J.-P.; Charlet, L.; Szenknect, S.; Barthès, V.; Krimissa, M. Sorption isotherms: A review on physical bases, modeling and measurement. *Appl. Geochem.* **2007**, *22*, 249−275.
(32) Johnson, J. B.; Omland, K. S. Model selection in ecology and evolution. *Trends Ecol. Evol.* **2004**, *19*, 101−108.
(33) Rajahmundry, G. K.; Garlapati, C.; Kumar, P. S.; Alwi, R. S.; Vo, D.-V. N. Statistical analysis of adsorption isotherm models and its appropriate selection. *Chemosphere* **2021**, *276*, 130176.
(34) Turner, B. D.; Henley, B. J.; Sleap, S. B.; Sloan, S. W. Kinetic model selection and the Hill model in geochemistry. *Int. J. Environ. Sci. Technol.* **2015**, *12*, 2545−2558.
(35) Bhatti, M. S.; Kapoor, D.; Kalia, R. K.; Reddy, A. S.; Thukral, A. K. RSM and ANN modeling for electrocoagulation of copper from simulated wastewater: Multi objective optimization using genetic algorithm approach. *Desalination* **2011**, *274*, 74−80.
(36) Jang, J.-S. R. ANFIS: adaptive-network-based fuzzy inference system. *IEEE Trans. Syst. Man Cybern.* **1993**, *23*, 665−685.
(37) Bingöl, D.; Inal, M.; Çetintaş, S. Evaluation of Copper Biosorption onto Date Palm (Phoenix dactylifera L.) Seeds with MLR and ANFIS Models. *Ind. Eng. Chem. Res.* **2013**, *52*, 4429−4435.
(38) Bhowmik, M.; Debnath, A.; Saha, B. Fabrication of mixed phase CaFe2O4 and $MnFe_2O_4$ magnetic nanocomposite for enhanced and rapid adsorption of methyl orange dye: statistical modeling by neural network and response surface methodology. *J. Dispers Sci. Technol.* **2020**, *41*, 1937−1948.
(39) Bhowmik, M.; Debnath, A.; Saha, B. Fabrication of mixed phase calcium ferrite and zirconia nanocomposite for abatement of methyl orange dye from aqua matrix: Optimization of process parameters. *Appl. Organomet. Chem.* **2018**, *32*, No. e4607.

https://doi.org/10.1021/acsomega.1c03964
ACS Omega 2021, 6, 30499−30514